Received: 17 February 2022 | Revised: 30 August 2022 | Accepted: 6 September 2022

DOI: 10.1002/col.22824

RESEARCH ARTICLE

COLOR RESEARCH AND APPLICATION WILEY

Appearance estimation and reconstruction of glossy object surfaces based on the dichromatic reflection model

Shoji Tominaga[1,2] | **Roseline Kim Fong Yong**[3]

[1]Department of Computer Science, Norwegian University of Science and Technology, Gjøvik, Norway

[2]Department of Business and Informatics, Nagano University, Ueda, Japan

[3]Department of Environmental Health Science and Public Health, Akita University Graduate School of Medicine, Akita, Japan

Correspondence
Shoji Tominaga, Department of Computer Science, Norwegian University of Science and Technology, Gjøvik, Norway.
Email: shojitominaga12@gmail.com

Funding information
Japan Society for the Promotion of Science KAKENHI, Grant/Award Number: JP20K11893

Abstract

We propose an approach for estimating and reconstructing the material appearance of objects based on the spectral image data acquired in complex illumination environments with multiple light sources. The object appearance can be constructed with various material properties such as spectral reflectance, glossiness, and matteness under different geometric and spectral illumination conditions. The objects are assumed to be made of an inhomogeneous dielectric material with gloss or specularity. The color signals from the object surface are described by the standard dichromatic reflection model, which consists of diffuse and specular reflections, where the specular component has the same spectral composition as the illuminant. The overall appearance of objects is determined by a combination of chromatic factors, based on the reflectance and illuminant spectra, and shading terms, which represent the surface geometries of the surface illumination. Therefore, the appearance of a novel object can be reconstructed by modifying the chromatic factors and shading terms. The method for appearance estimation and reconstruction comprises four steps: (1) illuminant estimation, (2) spectral reflectance estimation, (3) shading term estimation and region segmentation, and (4) appearance reconstruction based on the reflection model. The proposed approach is validated in an experiment in which objects of different materials are illuminated using different light sources. We demonstrate typical reconstruction results with novel object appearances.

KEYWORDS

appearance estimation and reconstruction, dichromatic reflection model, glossy surface, material appearance

1 | INTRODUCTION

Reconstruction of the appearance of objects with different material properties, such as color and gloss, under different illumination colors, or from different illumination directions, is often necessary in daily life settings. The creation of plausible novel object appearances under different conditions is called material object recoloring,[1,2]

appearance control,[3–5] or appearance editing.[6] Previous studies have used a three-dimensional (3D) color space as the control space for the appearance reconstruction of color images.

This study considers an approach for estimating and reconstructing the surface appearance of an object based on the spectral image data acquired in a complex illumination environment with multiple light sources. The use of high-dimensional spectral spaces not only increases the accuracy of estimation and reconstruction but is also far more versatile than the use of color spaces. Object appearance can be constructed with various material properties such as spectral reflectance, glossiness, and matteness under different geometric and spectral illumination conditions.

The objects we target in this study are everyday objects, such as natural objects and man-made objects, which are assumed to be made of an inhomogeneous dielectric material with gloss or specularity. The spectral composition of the reflected light from the object surface, often called the color signal,[7] is decomposed into two additive components, diffuse (body) reflection and specular (interface) reflection. The specular reflection has the same spectral composition as the illuminant of the input light source to the object surface. A dichromatic reflection model describes this type of light reflection.[8,9] The color signal is expressed as a weighted sum of two spectral components: one is described by the product of the spectral reflectance and the illuminant spectrum, and the other is described by the illuminant spectrum only. Several materials, such as man-made products as plastics, paints, ceramics, vinyl, and tiles and such natural products as fruits, leaves, and wood with hard and thick surface layers have dichromatic reflection properties.[9–11] We note, however, that fruits and leaves with soft and thin surface layers have subsurface scattering like human skin. Such objects cannot be described using the dichromatic reflection model because the spectral component based on subsurface scattering is added to the two components. As well, the model does not apply to translucent objects.

Because the color signal in the dichromatic reflection model is described by the weighted sum of these two components, the overall appearance of objects in a scene is determined by a combination of (1) chromatic factors, based on the spectral reflectances and the illuminant spectra, and (2) geometric factors, based on the weighting coefficients of the two components. The geometric factors represent the geometries of the surface and lighting, which are called the shading terms in this article (see[12]). Therefore, novel appearances of objects can be constructed in the dichromatic reflection model by modifying the chromatic and geometric factors. Figure 1 presents an example of the appearance reconstruction of a glossy natural object. We used a red paprika as the object to test the appearance reconstruction by using different conditions. Figure 1A shows the original appearance of a red paprika observed under three light sources from different directions, namely, a LED light (upper source), a fluorescent light (right source), and an incandescent light (left source). We reconstructed the original appearance under two different conditions of spectral reflectance and illuminants. First, the spectral reflectance of the red paprika was changed to the spectral reflectance

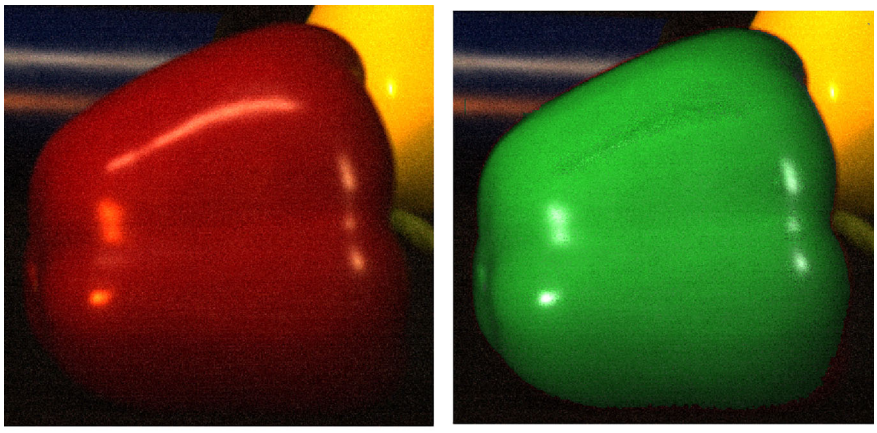

FIGURE 1 Example of appearance reconstruction of a glossy object: (A) original appearance of a red paprika observed under three light sources from different directions: a LED light (upper source), a fluorescent light (right source), and an incandescent light (left source). (B) Constructed appearance of the object under different conditions of material and illumination, where the object has the same surface geometries, but it has the surface reflectance of a green color checker and is illuminated according to CIE D65 from the right and left directions, except for the upper direction (see Section 6.6 for the details).

of a green paprika. Second, the light sources were changed to two light sources with different spectral power distributions. Figure 1B shows the constructed appearance of a green paprika with the same surface geometries, which has the reflectance of a green color sample and is illuminated according to CIE D65 from the right and left directions, except for the upper direction. The object appearance of paprika with different colors but same geometrics is reconstructed by replacing the spectral reflectance and the illuminant spectra with different spectral functions.

The basic process of reconstructing an object appearance requires estimating two types of spectral functions of surface reflectance for each object and scene illuminant and the shading terms from the spectral image data of the object acquired by a spectral imaging system. The method for appearance estimation and reconstruction proposed in this paper comprises four steps: (1) illuminant estimation, (2) spectral reflectance estimation, (3) shading term estimation and region segmentation, and (4) appearance reconstruction based on the reflection model.

Section 2 describes a simplified version of a previously proposed method for estimating multiple illuminants.[13] Multiple illuminants are estimated based on the highlight areas on the dielectric object surfaces. We suppose that the object surfaces are not flat but curved, and the light sources are located at different positions, far from the target objects. In such cases, each specular highlight area corresponds to only one light source among multiple light sources (see reference 13). If multiple illuminations with different spectral compositions may hit the same region on the object's surface, we treat such multiple light sources as a single light source. Highlight areas on the object surfaces are detected using a combination of Gaussian filters, and prominent highlight areas are selected for effective illuminant estimation. At a specular area on the object's surface, the reflected light is mixed with the diffuse reflection and specular reflection. When the target object's light reflection obeys the dichromatic reflection model, the specular reflection component has the same spectral composition as the light source. Therefore, we propose an algorithm to estimate the illuminant's spectral composition based on the dichromatic reflection model from the highlight area in the spectral image. The illuminant spectral curves are estimated from the pixel distributions in the respective highlight areas, which were further classified into groups of light sources to find a reliable set of illuminant estimates.

Section 3 proposes a comprehensive method for estimating the surface spectral reflectance based on the dichromatic reflection model. Spectral image data for a specific area will be selected from an object surface are described using the estimated illuminant spectra, surface spectral reflectance, and shading terms. This estimation is based on the fact that the two unknowns have different domains. The spectral reflectance will be defined in the wavelength domain, and the shading terms will be defined in the spatial coordinate domain. We develop an iterative algorithm that repeatedly estimates the reflectance and shading terms in two steps. The output estimates in the first step will be used as input in the second step, then the output estimate will feedback to the first step for iterative estimation.

In Section 4, we propose that the shading terms are estimated for a large area of the image based on the previously estimated illuminants and spectral reflectances. Then each object region is proposed to be segmented using the spectral angle (SA). First, a region suitable for describing the appearance of each object, such as a region with highlights and no boundaries or shadows, will be selected as a reference region, and the average color signal in that region will be calculated as a reference spectrum. The SA is to be defined to represent the spectral similarity between two vectors in the high-dimensional spectral space. Next, we will calculate the SA at each pixel between the reference spectrum and the original spectral image. Pixels with small SAs will then be grouped in the same material region. Thus, region segmentation will be performed based on spectral similarity.

In Section 5, novel appearances of objects in the original scene will be created by modifying some components of the reflection model in the respective segmented regions, where the spectral functions of reflectances and illuminants are replaced with different functions to reconstruct the color appearance as shown in Figure 1B. The shading intensities are changed to reconstruct the geometric appearance, such as matteness and glossiness. An inpainting technique will be used to correct the irregular areas in the estimated shading images. The entire procedure will be presented for appearance reconstruction.

In Section 6, the feasibility of the proposed approach will be examined in an experiment using everyday objects observed by a spectral imaging system in an illumination environment with multiple light sources. We plan to show the accuracies of both the estimated illuminant spectra of the light sources and the estimated surface spectral reflectances of the objects. We will calculate the root mean square errors (RMSEs) between the estimated color signals based on the dichromatic reflection model and the observed image data for a comprehensive accuracy assessment. We will then demonstrate typical reconstruction results with novel appearances of objects to confirm the feasibility of the proposed appearance estimation and reconstruction approach.

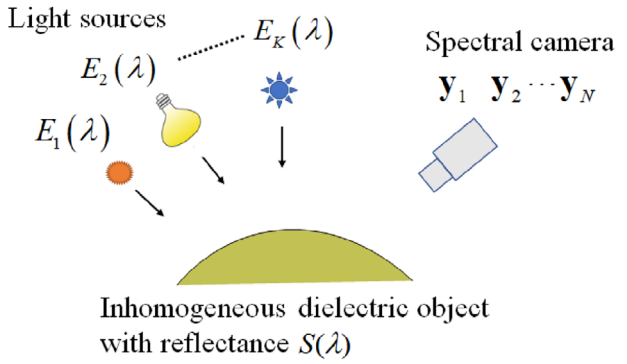

FIGURE 2 Scene of an inhomogeneous dielectric object observed by a spectral camera under multiple light sources

2 | ILLUMINANT ESTIMATION

The estimation process of the illuminant spectra of multiple light sources comprises two steps: (1) highlight detection and (2) spectral estimation. Here, we describe a simplified version of a previously proposed method for estimating multiple illuminants.[13]

2.1 | Highlight detection

Figure 2 shows a scene in which a spectral camera observes a target object composed of an inhomogeneous dielectric material under K multiple light sources. The inhomogeneous material is a substance composed of different component materials, such as a vehicle at the surface layer and embedded pigments at the colorant layer. For example, plastics and paints are inhomogeneous. Metals and crystals are typical examples of homogeneous objects (see reference 9). Let $Y(\lambda, \mathbf{x})$ be the observed color signal (spectral radiance of the reflected light) at wavelength λ and pixel location $\mathbf{x} = (x, y)$ from the object surface. Color signals can be recovered from the outputs of a spectral imaging system by determining the spectral sensitivity functions. We used the luminance value $L(\lambda)$ for highlight detection. To perform this, the original color image $Y(\lambda, \mathbf{x})$ was converted into the CIE-XYZ space using the CIE color-matching functions, and then the luminance component L was selected. Two Gaussian filters were applied to the luminance image $L(\lambda)$. One is the center-surround filter, which is determined by the difference of two Gaussian distributions (DOGs). A broader DOG has a large standard deviation σ_1 and a narrower DOG has a small standard deviation σ_2, where $\sigma_1 > \sigma_2$. The values for σ_1 and σ_2 are empirically chosen. For instance, the image in Figure 1 has a size of about 500×500. In such a case, σ_1 is chosen to about 10–15, and σ_2 is chosen to about 1/4–1/3 of σ_1. The broader DOG was subtracted from the narrower DOG, as shown in Figure 3A. This filter is effective for detecting specular highlight areas, as well as a boundary region between the objects and the background. The other filter is a low-pass filter of the DOG with a large standard deviation σ_3, as shown in Figure 3B. This other filter is used to remove the boundary regions. We select the highlights with strong intensities among the detected highlight areas by both filters. This is because the highlights with strong intensities are more effective in estimating the illumination than those with weak intensities, where the color signal of weak specular reflection is contaminated more by diffuse reflection from nearby objects.

2.2 | Spectral estimation

The detected highlight areas provide important clues for estimating the illuminant spectra. There are several constraints. Each object surface is supposed to be convex, curved, and smooth, not rough surfaces. Concerning light sources, multiple light sources are supposed to be separated from the target objects also separated from each other. In this situation, specular reflection occurs when the incident angle of incoming light to the surface coincides with the camera's viewing angle. Each detected highlight area on the surface has illuminant spectral information (SI) of the corresponding one light source among the multiple light sources. If the light sources overlap, they are treated as one light source.

We assume L different light sources. Let $S(\lambda)$ be the surface spectral reflectance of the target object, and let $E(\lambda)$ be the spectral power distribution of the incident light, which is a mixture of different illuminants from K light sources, $E(\lambda) = E_1(\lambda) + E_2(\lambda) + \ldots + E_K(\lambda)$. Then, the color signal observed at highlight point $\mathbf{x}_\mathrm{p}$ is described as

$$Y(\lambda, \mathbf{x}_\mathrm{p}) = c_\mathrm{S}(\mathbf{x}_\mathrm{p}) E_p(\lambda) + c_\mathrm{D}(\mathbf{x}_\mathrm{p}) S(\lambda) E(\lambda), \qquad (1)$$

where the first and second terms represent the specular and diffuse reflection components, respectively. The spectral function $E_p(\lambda)$ is the illuminant spectrum of a single light source corresponding to the highlight. The weighting coefficients of the spectral functions, $c_\mathrm{S}(\mathbf{x}_\mathrm{p})$ and $c_\mathrm{D}(\mathbf{x}_\mathrm{p})$, are constants over the visible wavelength range. We estimate $E_p(\lambda)$ based on the dataset of observed spectra $\{Y(\lambda, \mathbf{x}_\mathrm{p})\}$ in the highlight area.

To make the calculation of illuminant estimation easier, we use the discrete representation of color signals.

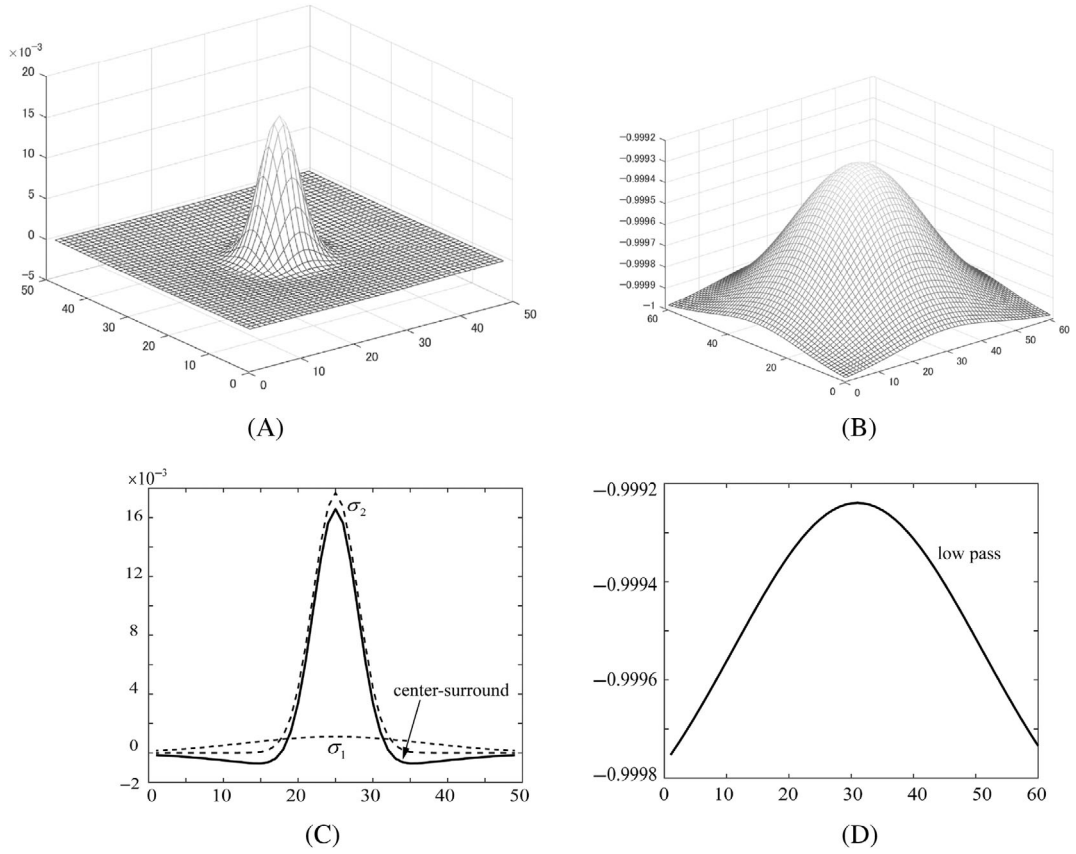

FIGURE 3 Typical filter shapes of (A) the center-surround filter ($\sigma_1 = 12$, $\sigma_2 = 3$) and (B) the low pass filter ($\sigma_3 = 20$), and also 2D side views (C) and (D) corresponding to (A) and (B), respectively, where the shape difference is clearly seen.

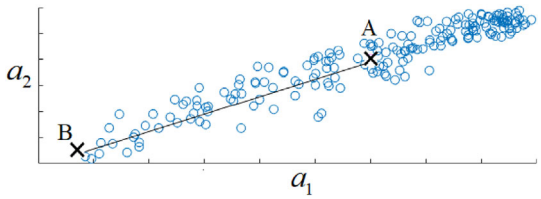

FIGURE 4 Pixel distribution of the image data in a highlight area projected on the two-dimensional space (a_1, a_2), where points A and B are the centroid of the pixel distribution and the farthest pixel point from the centroid A, respectively.

Let $\mathbf{y}$ be an n-dimensional vector of the color signal $Y(\lambda, \mathbf{x})$ in the highlight area when the visible range (400–700 nm) is sampled at n wavelengths with equal intervals. Typically, all spectral functions are sampled in the high dimension of $n = 61$ at 5 nm intervals in this study. Because the color signal is expressed as a linear combination of only two spectral components, the color signal has two-dimensionality. Therefore, the image data in highlight area are projected onto a two-dimensional subspace spanned by two principal components. Let $\mathbf{p}_1$ and $\mathbf{p}_2$ be the first and second principal components, calculated using principal component analysis for a dataset of the color signals in the highlight area. The projection from the n-dimensional space to the two-dimensional subspace is described as

$$\begin{bmatrix} a_1 \\ a_2 \end{bmatrix} = \begin{bmatrix} \mathbf{p}_1{}^t \\ \mathbf{p}_2{}^t \end{bmatrix} \mathbf{y}, \tag{2}$$

where symbol t indicates matrix transposition.

Figure 4 shows an example of the pixel distribution of the image data projected onto the two-dimensional subspace. The pixel distribution on the coordinate (a_1, a_2) consists of two clusters. The pixel distribution in the upper right in the figure mostly belongs to the cluster by the diffuse reflection component, and the remaining linear distribution is the cluster by the specular reflection component. Because the specular component has the illuminant spectral composition, the directional vector of this linear cluster corresponds to the light source color, that is, the illumination to be estimated. In Figure 4, points A and B are the centroid of the pixel distribution and the farthest pixel point from the centroid A, respectively. Let the directional vector $\mathrm{A} \rightarrow \mathrm{B}$ be (a_1', a_2'). Then the illuminant vector $\mathbf{E}$ of the spectral function $E_p(\lambda)$ can be estimated by

transforming (a'_1, a'_2) into the n-dimensional spectral space as follows:

$$\widehat{\mathbf{E}} = \begin{bmatrix} \mathbf{p}_1{}^t \\ \mathbf{p}_2{}^t \end{bmatrix}^+ \begin{bmatrix} a'_1 \\ a'_2 \end{bmatrix}, \tag{3}$$

where symbol + indicates the generalized inverse of a matrix.

Because the estimates contain errors, we classified the estimated spectral curves into groups of light sources to find a reliable set of illuminant estimates. We adopt the k-means clustering algorithm[14] to perform this grouping. The algorithm has an iterative process, where it starts with initial estimates for the K centroids of illuminants, which are randomly selected from the spectral dataset. Each data point is assigned to its nearest centroid based on Euclidean distance (ED). The centroid is recalculated for each cluster. Because the number of light sources is known in advance, we can set parameter K to the number of light sources L.

If the number L of light sources is unknown, we cannot set K to L in advance. In this case, the parameter K changes based on the number of detected highlights. Therefore, the classification result depends on largely on the initial values for K centroids. As the first step, we repeat the clustering algorithm by changing the initial values randomly. So that we have a set of classified illuminant spectra for different classes of K. We note that classification using only the estimated spectra is not enough to identify the light sources on each object surface.

As the second step, we assign the most matched illuminant to each detected highlight location on each object surface, since specular highlights appear on multiple objects in the scene. The highlight locations on each surface are closely related to the relative directions to where those light sources exist. For example, when the object surfaces are convex, the highlight position on the left suggests that the light source is located left, and the light comes from the left direction. Thus, the relative positional relationship between highlight areas among different object surfaces is useful for identifying spectral light sources on each surface. We use not only the illuminant SI but also highlight locational information. The method of probabilistic relaxation labeling can be applied to solving the present identification problem. The details of this method are shown in,[13] where the results illustrating the critical choice of K are demonstrated. Thus, a set of reliable illuminant estimates can be determined by examining the best match based on the positional relationship among the light source candidates detected from the highlights of multiple object surfaces.

3 | REFLECTANCE ESTIMATION

3.1 | Model equations

We consider the estimation of spectral reflectance $S(\lambda)$. A discrete form of the color signal $Y(\lambda, \mathbf{x})$ is often represented as an n-dimensional column vector when the visible range (400–700 nm) is sampled at n wavelengths with equal intervals. Let N be the number of pixels in the region of interest (ROI). The color signals observed at wavelengths λ_i (i = 1, 2, ..., n) and pixel points $\mathbf{x}_j$ (j = 1, 2, ..., N) are described as follows:

$$\begin{aligned} Y(\lambda_i, \mathbf{x}_j) = {} & c_{S1}(\mathbf{x}_j) E_1(\lambda_i) + c_{S2}(\mathbf{x}_j) E_2(\lambda_i) + \ldots \\ & + c_{SK}(\mathbf{x}_j) E_K(\lambda_i) + c_{D1}(\mathbf{x}_j) S(\lambda_i) E_1(\lambda_i) \\ & + c_{D2}(\mathbf{x}_j) S(\lambda_i) E_2(\lambda_i) + \ldots \\ & + c_{DK}(\mathbf{x}_j) S(\lambda_i) E_K(\lambda_i), \end{aligned} \tag{4}$$

where the first K terms represent the specular reflection by the illumination of L light sources, and the latter K terms represent the diffuse reflection by illumination of the same light sources. The weighting coefficients $c_{Sk}(\mathbf{x}_j)$ and $c_{Dk}(\mathbf{x}_j)$ (k = 1, 2, ..., K) are shading terms, which depend on geometries such as object shape, position, and distance from the light source and camera. Normally, there are as many shading terms as there are two components of specular reflection and diffuse reflection multiplied by the number of light sources.

We note that the illuminant spectra $E_k(\lambda)$ (k = 1, 2, ..., K) of K light sources have already been estimated as described in the previous section, so we denote the estimate by $\widehat{E}_k(\lambda)$. The spectral reflectance $S(\lambda)$ and shading terms $c_{Sk}(\mathbf{x}_j)$ and $c_{Dk}(\mathbf{x}_j)$ (k = 1, 2, ..., K) are unknown. We define several vectors for the discrete representation of the model as follows:

$$\mathbf{s} = \begin{bmatrix} S(\lambda_1) \\ S(\lambda_2) \\ \vdots \\ S(\lambda_n) \end{bmatrix}, \quad \mathbf{y}_j = \begin{bmatrix} Y(\lambda_1, \mathbf{x}_j) \\ Y(\lambda_2, \mathbf{x}_j) \\ \vdots \\ Y(\lambda_n, \mathbf{x}_j) \end{bmatrix}, \quad \mathbf{c}_j = \begin{bmatrix} c_{S1}(\mathbf{x}_j) \\ \vdots \\ c_{SK}(\mathbf{x}_j) \\ c_{D1}(\mathbf{x}_j) \\ \vdots \\ c_{DK}(\mathbf{x}_j) \end{bmatrix},$$

$$\mathbf{z}_i = \begin{bmatrix} Y(\lambda_i, \mathbf{x}_1) - c_{S1}(\mathbf{x}_1)\widehat{E}_1(\lambda_i) - c_{S2}(\mathbf{x}_1)\widehat{E}_2(\lambda_i) - \ldots - c_{SL}(\mathbf{x}_1)\widehat{E}_L(\lambda_i) \\ Y(\lambda_i, \mathbf{x}_2) - c_{S1}(\mathbf{x}_2)\widehat{E}_1(\lambda_i) - c_{S2}(\mathbf{x}_2)\widehat{E}_2(\lambda_i) - \ldots - c_{SL}(\mathbf{x}_2)\widehat{E}_L(\lambda_i) \\ \vdots \\ Y(\lambda_i, \mathbf{x}_N) - c_{S1}(\mathbf{x}_N)\widehat{E}_1(\lambda_i) - c_{S2}(\mathbf{x}_N)\widehat{E}_2(\lambda_i) - \ldots - c_{SL}(\mathbf{x}_N)\widehat{E}_K(\lambda_i) \end{bmatrix},$$
$$(i = 1, 2, \ldots, n, \ j = 1, 2, \ldots, N) \tag{5}$$

where $\mathbf{s}$ is an n-dimensional column vector of the spectral reflectance; $\mathbf{y}_j$ is an n-dimensional column vector of the imaging system output at location (pixel point) $\mathbf{x}_j$, $\mathbf{c}_j$ is a 2 K-dimensional column vector of the shading terms at location $\mathbf{x}_j$, and $\mathbf{z}_i$ is an N-dimensional observation vector for the diffuse reflection component at wavelength λ_i, which is obtained by subtracting the specular reflection component from the observation.

3.2 | Estimation algorithm

There are two types of unknown variables: $\mathbf{s}$ and $\mathbf{c}_j$, which have different domains. The spectral reflectance is defined in the wavelength domain, and the shading terms are defined in the spatial coordinate domain. Utilizing this property, we propose an iterative solution method to obtain the optimal estimates of the surface spectral reflectance function and all the weighting coefficients of the shading terms. The iterative process is decomposed into two steps: (1) the estimates of the shading terms are updated under the estimated reflectance fixed, and (2) the estimate of the spectral reflectance is updated under the estimated shading terms fixed.

3.2.1 | Shading term estimation

The relationship between the shading terms and all observations is described as

$$\begin{bmatrix}\mathbf{y}_1\\ \mathbf{y}_2\\ \vdots\\ \mathbf{y}_N\end{bmatrix}=\begin{bmatrix}\mathbf{B} & \mathbf{0} & \cdots & \mathbf{0}\\ \mathbf{0} & \mathbf{B} & \ddots & \vdots\\ \vdots & \ddots & \ddots & \mathbf{0}\\ \mathbf{0} & \cdots & \mathbf{0} & \mathbf{B}\end{bmatrix}\begin{bmatrix}\mathbf{c}_1\\ \mathbf{c}_2\\ \vdots\\ \mathbf{c}_N\end{bmatrix}, \tag{6}$$

where the observation vector on the left side is a high dimensional vector with n*N dimensions, and an $n \times 2$ K matrix $\mathbf{B}$ on the right side is defined as

$$\mathbf{B}=\begin{bmatrix}\widehat{E}_1(\lambda_1) & \widehat{E}_2(\lambda_1) & \cdots & \widehat{E}_K(\lambda_1) & S(\lambda_1)\widehat{E}_1(\lambda_1) & S(\lambda_1)\widehat{E}_2(\lambda_1) & \cdots & S(\lambda_1)\widehat{E}_K(\lambda_1)\\ \widehat{E}_1(\lambda_2) & \widehat{E}_2(\lambda_2) & \cdots & \widehat{E}_K(\lambda_2) & S(\lambda_2)\widehat{E}_1(\lambda_2) & S(\lambda_2)\widehat{E}_2(\lambda_2) & \cdots & S(\lambda_2)\widehat{E}_K(\lambda_2)\\ \vdots & \vdots & & \vdots & \vdots & \vdots & & \vdots\\ \widehat{E}_1(\lambda_n) & \widehat{E}_2(\lambda_n) & \cdots & \widehat{E}_K(\lambda_n) & S(\lambda_n)\widehat{E}_1(\lambda_n) & S(\lambda_n)\widehat{E}_2(\lambda_n) & \cdots & S(\lambda_n)\widehat{E}_K(\lambda_n)\end{bmatrix}. \tag{7}$$

The observation at each pixel point is rewritten as

$$\mathbf{y}_j=\mathbf{B}\mathbf{c}_j\ (j=1,2,...,N). \tag{8}$$

Therefore, the standard least square estimate for $\mathbf{c}_j$ is given in a form

$$\widehat{\mathbf{c}}_j=(\mathbf{B}^t\mathbf{B})^{-1}\mathbf{B}^t\mathbf{y}_j\ (j=1,2,...,N). \tag{9}$$

3.2.2 | Spectral reflectance estimation

The relationship between the spectral reflectance and all observations is described as

$$\begin{bmatrix}\mathbf{z}_1\\ \mathbf{z}_2\\ \vdots\\ \mathbf{z}_n\end{bmatrix}=\begin{bmatrix}\mathbf{b}_1 & \mathbf{0} & \cdots & \mathbf{0}\\ \mathbf{0} & \mathbf{b}_2 & \ddots & \vdots\\ \vdots & \ddots & \ddots & \mathbf{0}\\ \mathbf{0} & \cdots & \mathbf{0} & \mathbf{b}_n\end{bmatrix}\begin{bmatrix}S(\lambda_1)\\ S(\lambda_2)\\ \vdots\\ S(\lambda_n)\end{bmatrix}, \tag{10}$$

where the observation vector on the left side is an N*n-dimensional vector, and the $n \times 1$ matrix $\mathbf{b}_i$ on the right side is defined as

$$\mathbf{b}_i=\begin{bmatrix}c_{D1}(\mathbf{x}_1)\widehat{E}_1(\lambda_i)+c_{D2}(\mathbf{x}_1)\widehat{E}_2(\lambda_i)+\cdots+c_{DL}(\mathbf{x}_1)\widehat{E}_K(\lambda_i)\\ c_{D1}(\mathbf{x}_2)\widehat{E}_1(\lambda_i)+c_{D2}(\mathbf{x}_2)\widehat{E}_2(\lambda_i)+\cdots+c_{DL}(\mathbf{x}_2)\widehat{E}_K(\lambda_i)\\ \vdots\\ c_{D1}(\mathbf{x}_N)\widehat{E}_1(\lambda_i)+c_{D2}(\mathbf{x}_N)\widehat{E}_2(\lambda_i)+\cdots+c_{DL}(\mathbf{x}_N)\widehat{E}_K(\lambda_i)\end{bmatrix}. \tag{11}$$

The observation at each wavelength is rewritten as

$$\mathbf{z}_i=\mathbf{b}_iS(\lambda_i)\ (i=1,2,...,n). \tag{12}$$

Therefore, the standard least square estimate for $\mathbf{s}$ is given in a form

$$\widehat{S}(\lambda_i)=\mathbf{b}_i^t\mathbf{z}_i/\left(\mathbf{b}_i^t\mathbf{b}_i\right)\ (i=1,2,...,n), \tag{13}$$

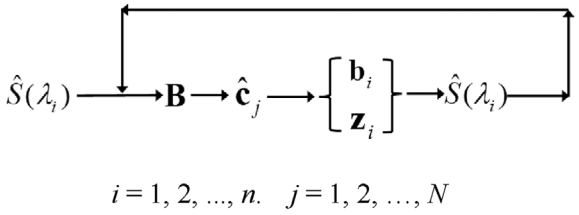

FIGURE 5 Visual diagram of the iterative process for reflectance estimation

where we note that the estimate is a scalar.

3.2.3 | Iterative estimation process

We repeat the iterative estimation calculations of the above steps (1) and (2), starting from an appropriate initial estimate of spectral reflectance. Figure 5 shows a visual diagram of the iterative estimation process. The initial value of $\widehat{S}(\lambda_i)$ is constant in the range $400 \le \lambda \le 700$ (say, $\widehat{S}(\lambda_i) = 0.5$).

In the observation model above, Equation (4), the shading term $c_{Dk}(\mathbf{x})$ (k = 1, 2, ..., K) and spectral reflectance $S(\lambda)$ are multiplied by $c_{Dk}(\mathbf{x})S(\lambda)$. In this case, the absolute value of each estimate could not be determined. For instance, if the shading term is doubled as $2c_{Dk}(\mathbf{x})$ and the spectral reflectance is halved as $S(\lambda)/2$, the multiplication is the same. Therefore, we assume that the spectral reflectance is normalized by $\sum_{i=1}^{n} S(\lambda_i)^2 = 1$ ($\|\mathbf{s}\| = 1$) in this iterative process.

The area selected for reflectance estimation may affect performance. Because we aim to estimate the spectral reflectance for the diffuse reflection component, only matte areas that contain neither gloss nor specularity can be extracted and used for estimation. In this case, the specular shading terms $c_{Sk}(\mathbf{x})E_k(\lambda)$ (k = 1, 2, ..., K) in the above algorithm are neglected as $c_{Sk}(\mathbf{x}) = 0$, so that we have

$$\mathbf{c}_j = \begin{bmatrix} c_{D1}(\mathbf{x}_j) \\ c_{D2}(\mathbf{x}_j) \\ \vdots \\ c_{DK}(\mathbf{x}_j) \end{bmatrix}, \quad \mathbf{z}_i = \begin{bmatrix} Y(\lambda_i, \mathbf{x}_1) \\ Y(\lambda_i, \mathbf{x}_2) \\ \vdots \\ Y(\lambda_i, \mathbf{x}_N) \end{bmatrix}. \quad (i = 1, 2, ..., n, \ j = 1, 2, ..., N). \tag{14}$$

4 | SHADING TERM ESTIMATION AND REGION SEGMENTATION

4.1 | Shading term estimation

Shading term estimation in the previous section was applied to a limited region of the image for reflectance estimation. Shading estimation in this section is expanding the region to the whole image. The shading terms are estimated at all pixel points in a wide area, including the target object, based on the previously estimated illuminants and spectral reflectance. For this purpose, let $\mathbf{y}(\mathbf{x}_j)$ and $\mathbf{c}(\mathbf{x}_j)$ be the observed color signal vector and the shading terms at pixel point $\mathbf{x}_j$ (j = 1, 2, ..., N), respectively. The observational model in Equation (4) can be expressed as

$$\begin{aligned} \mathbf{y}(\mathbf{x}_j) &= c_{S1}(\mathbf{x}_j)\widehat{\mathbf{e}}_1 + c_{S2}(\mathbf{x}_j)\widehat{\mathbf{e}}_2 + ... + c_{SK}(\mathbf{x}_j)\widehat{\mathbf{e}}_K \\ &\quad + c_{D1}(\mathbf{x}_j)\widehat{\mathbf{s}}.*\widehat{\mathbf{e}}_1 + c_{D2}(\mathbf{x}_j)\widehat{\mathbf{s}}.*\widehat{\mathbf{e}}_2 + ... + c_{DK}(\mathbf{x}_j)\widehat{\mathbf{s}}.*\widehat{\mathbf{e}}_K \\ &= [\widehat{\mathbf{e}}_1 \ \ \widehat{\mathbf{e}}_2 \ \ \cdots \ \ \widehat{\mathbf{e}}_K \ \ \widehat{\mathbf{s}}.*\widehat{\mathbf{e}}_1 \ \ \widehat{\mathbf{s}}.*\widehat{\mathbf{e}}_2 \ \ \cdots \ \ \widehat{\mathbf{s}}.*\widehat{\mathbf{e}}_K]\mathbf{c}(\mathbf{x}_j), \\ &\quad (j = 1, 2, ..., N) \end{aligned} \tag{15}$$

where $\widehat{\mathbf{s}}$ and $\widehat{\mathbf{e}}_k$ (k = 1, 2, ..., K) are the estimated spectral functions of the reflectance and illuminant, respectively. The symbol (. *) represents element-wise multiplication. For mathematical simplicity, when we define an $n \times 2L$ matrix $\mathbf{A}$ as

$$\mathbf{A} = [\widehat{\mathbf{e}}_1 \ \ \widehat{\mathbf{e}}_2 \ \ \cdots \ \ \widehat{\mathbf{e}}_K \ \ \widehat{\mathbf{s}}.*\widehat{\mathbf{e}}_1 \ \ \widehat{\mathbf{s}}.*\widehat{\mathbf{e}}_2 \ \ \cdots \ \ \widehat{\mathbf{s}}.*\widehat{\mathbf{e}}_K], \tag{16}$$

we have

$$\mathbf{y}(\mathbf{x}_j) = \mathbf{A}\mathbf{c}(\mathbf{x}_j) \ (j = 1, 2, ..., N). \tag{17}$$

As the shading terms always take nonnegative values, we solve a least-squares problem to find the $\mathbf{c}(\mathbf{x}_j)$ that minimizes the residual norm $\|\mathbf{y}(\mathbf{x}_j) - \mathbf{A}\mathbf{c}(\mathbf{x}_j)\|_2^2$ subject to $\mathbf{c}(\mathbf{x}_j) \ge 0$. In this study, we adopt the MATLAB function "lsgnoneq" to solve this nonnegative linear least-squares problem. The obtained estimate $\widehat{\mathbf{c}}(\mathbf{x}_j)$ is a $2L$ dimensional vector, where the first K elements $\widehat{c}_1(\mathbf{x}_j)$, $\widehat{c}_2(\mathbf{x}_j)$, ..., $\widehat{c}_K(\mathbf{x}_j)$ and the latter ..., $\widehat{c}_{K+1}(\mathbf{x}_j)$, ..., $\widehat{c}_{K+2}(\mathbf{x}_j)$, ..., $\widehat{c}_{2K}(\mathbf{x}_j)$ correspond to the shading terms for the specular reflection and diffuse reflection by the K illuminants, respectively.

4.2 | Region segmentation

Region segmentation extracts an area belonging to the same material among the observed image. The region segmentation technique looks for similarities between the pixels. In other words, pixels with similar attributes are grouped into a unique region. Because our image data are high-dimensional spectra, we consider a region-segmentation technique based on spectral features.

The estimated spectral reflectance is an important feature for region segmentation. However, the experimental results suggest that the color signals predicted using the estimated spectral reflectances and illuminants are more suitable than the spectral reflectances for segmenting regions of the object surfaces with specular reflection and gloss. Hereby, we propose the steps for the use of color signals for region segmentation. First, a region suitable for representing each object appearance is chosen as the reference region. In practice, we select a wide region on each object surface that includes all high light areas but excludes boundary and dark shadow areas. Then, the average of the predicted color signals in that region is calculated as a reference color signal.

Next, we consider region segmentation based on the material properties. Traditionally, various spectral similarity measures were proposed to be used to classify high-dimensional image data captured by a spectral imaging system in the fields, including remote sensing. The representative measures are the SA, the Euclidean distance (ED), the spectral frequency spectrum difference (SFSD), the spectral correlation (SC), the spectral gradient (SG), and the spectral information (SI (see references 15–19). From the viewpoint of dealing with the material appearance of strong glossy objects, the ED and SC measures are not available for dichromatic surfaces but only available for smooth diffuse surfaces. The SFSD and SI measures have high computational costs because of transformation into frequency domain and calculating random variables with a probability distribution. The SA is a based on the measurement of the spectral similarity between two spectral vectors. It is invariant with respect to the lengths of the spectral vectors, and effectively represses the influence of shading on object surface. Although SC is similar to SA, the SA is more direct and simpler. Thus, we adopt the SA to predict the spectral similarity between two vectors in a high-dimensional space in this paper.

The basic formula for the SA is defined as follows:

$$\theta = \cos^{-1}\left(\frac{\mathbf{y}_1^t \cdot * \mathbf{y}_2}{\|\mathbf{y}_1\|\|\mathbf{y}_2\|}\right), \tag{18}$$

where the symbol $\|\mathbf{y}\|$ indicates the norm $\mathbf{y}$. The angle θ represents the spectral similarity of $\mathbf{y}_1$ and $\mathbf{y}_2$: as the SA decreases, the two vectors become more similar. The angle ranges from 0° to 90°.

In the present region segmentation, we can assign $\mathbf{y}_1$ and $\mathbf{y}_2$ to the reference color signal $\mathbf{y}_{\text{ref}}$ and color signal $\mathbf{y}(\mathbf{x}_j)$, respectively, in the acquired spectral image. Therefore, we have

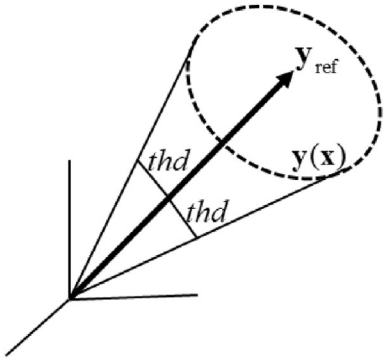

FIGURE 6 Principle of region segmentation based on the SA between the reference and color signals in the acquired image. If the SA between the two vectors $\mathbf{y}_{\text{ref}}$ and $\mathbf{y}(\mathbf{x}_j)$ is less than or equal to the threshold, the pixel of $\mathbf{x}_j$ is added to the same region. The threshold value *thd* is chosen empirically in the range (0°, 90°). In our experiments, we set *thd* = 30.

$$\theta = \cos^{-1}\left(\frac{\mathbf{y}_{\text{ref}}^t \cdot * \mathbf{y}(\mathbf{x}_j)}{\|\mathbf{y}_{\text{ref}}\|\|\mathbf{y}(\mathbf{x}_j)\|}\right). \tag{19}$$

The reference color signal is the average of the predicted color signals over the reference region and is calculated as follows:

$$\mathbf{y}_{\text{ref}} = \sum_{j=1}^{N} \hat{\mathbf{y}}(x_j)/N = \sum_{j=1}^{N} \mathbf{A}\hat{\mathbf{c}}(x_j)/N. \tag{20}$$

The SA θ is not affected by the illumination intensity because the angle between the two spectral vectors is independent of the norm of the vectors.

The present segmentation method is simplified because the similarity between adjacent pixels is not considered, and only the angle similarity between the reference and original color signals is considered. Figure 6 illustrates the simplified region segmentation using the SA in the 3D space. The observed color signals $\mathbf{y}(\mathbf{x}_j)$ in the image are compared with the reference color $\mathbf{y}_{\text{ref}}$. If the SA between the two vectors is less than or equal to the threshold, that is, $\theta \le thd$, the pixel of $\mathbf{x}_j$ is added to the same region.

5 | APPEARANCE RECONSTRUCTION

5.1 | Inpainting of the estimated shading terms

Different appearances of objects in the original scene can be reconstructed by modifying certain components of the

dichromatic reflection model in the respective segmented regions. The shading image of the reconstructed appearance is based on the estimated shading terms in each segmented region. As shown in the experimental results in the following section, an error often occurs when estimating the shading terms for the diffuse reflection component in an area where strong specular reflection occurs.

Figure 7A shows the image of the estimated shading terms $\hat{c}_{D2}(\mathbf{x}_j)$ for the second diffuse reflection component when the spectral image in Figure 1A is decomposed into three components according to the three illuminants. The areas of the dark holes correspond to the strong highlight areas. These errors are caused by the large intensity difference between the specular and diffuse reflections. An image inpainting technique is applied to reconstruct the irregular holes in the image. We adopt the MATLAB function "clickCallback" to perform inpainting interactively, where the selected irregular area is corrected using the exemplar-based matching method (see reference 20). We specify a limited area, including the irregular holes, and interactively perform inpainting for all irregular holes while checking the correction. Figure 7B shows an image corrected using the inpainting technique. In comparison between Figure 7A,B, artifacts look to appear at the place of the top highlights since the inpainting is not always perfect.

5.2 | Appearance reconstruction algorithm

The novel appearance of objects in the original scene is created by modifying some components of the reflection model in the segmented region for each object. The appearance reconstruction algorithm based on the dichromatic reflection model is described as follows:

$$\mathbf{y}(\mathbf{x}_j) = \hat{c}_{S1}(\mathbf{x}_j)\mathbf{e}_1 + \hat{c}_{S2}(\mathbf{x}_j)\mathbf{e}_2 + \ldots + \hat{c}_{SK}(\mathbf{x}_j)\mathbf{e}_K + \hat{c}_{D1}(\mathbf{x}_j)\mathbf{s}.*\mathbf{e}_1 + \hat{c}_{D2}(\mathbf{x}_j)\mathbf{s}.*\mathbf{e}_2 + \ldots + \hat{c}_{DK}(\mathbf{x}_j)\mathbf{s}.*\mathbf{e}_K. \quad (21)$$

Figure 8 shows the algorithm flow for the appearance reconstruction based on the estimated spectral functions and shading terms, where the broken lines represent the flow for appearance estimation of the observed image. We can change the illuminant spectra $\mathbf{e}_i$ ($i = 1, 2, \ldots, K$) of multiple light sources and the surface spectral reflectance $\mathbf{s}$ of the target object to the other spectral functions of illuminant and reflectance, so that chromatic appearances, such as object color, are reconstructed. More

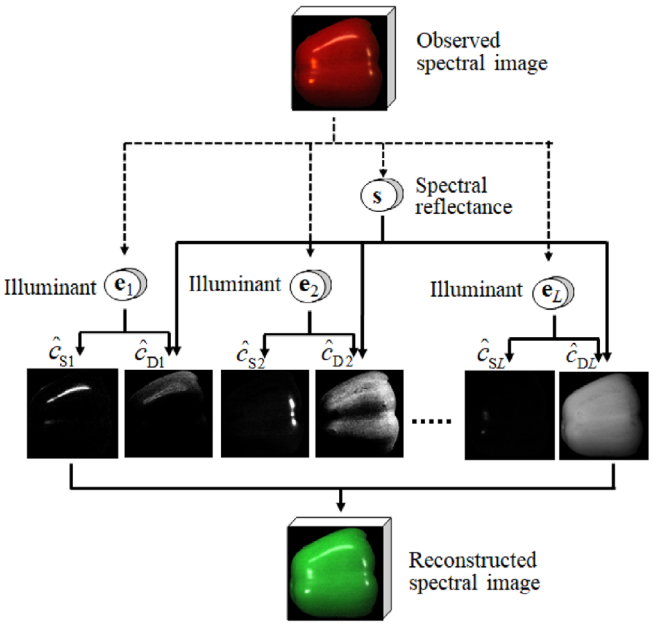

FIGURE 8 Algorithm flow for appearance reconstruction

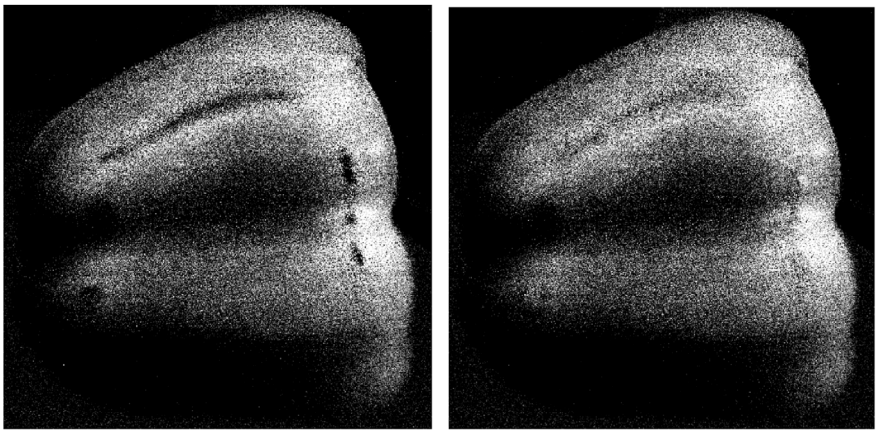

(A) (B)

FIGURE 7 Example of inpainting for an image with irregular holes: (A) original shading image with areas of dark holes, which is estimated for the shading terms of the second diffuse reflection component in decomposition of the spectral image in Figure 1A, (B) image is corrected for the irregular holes using an inpainting technique.

specifically, the object color is changed mainly by spectral reflectance, and the illuminant spectra change the illuminant environment. These spectral functions can be freely obtained from reflectance and illumination databases. For the convenience of processing, the illuminants are normalized using $\|\mathbf{e}_i\| = 1$.

It should be noted that the light source positions are fixed and independent of the object appearance. The geometric appearance of the object surfaces is mainly controlled based on shading terms. If we do not require a specific light source i, we simply set $\hat{c}_{Si}(\mathbf{x}_j) = \hat{c}_{Di}(\mathbf{x}_j) = 0$ or $\mathbf{e}_i = 0$. For instance, in Figure 1B, the upper light source among the three light sources is removed. To create a matte surface without specularity, we set all specular shading terms to $\hat{c}_{Si}(\mathbf{x}_j) = 0$ $(i = 1, 2, ..., K)$. In addition, the degree of matteness or glossiness can be controlled by adjusting the intensities of the specular and diffuse shading terms $(\hat{c}_{Si}(\mathbf{x}_j), \hat{c}_{Di}(\mathbf{x}_j))$. Thus, a wide variety of appearance editing techniques can be performed, except for the addition of a light source.

6 | EXPERIMENTAL RESULTS

6.1 | Experimental setup and model validation

A spectral imaging system was used in the experiments, which consisted of a monochrome CCD camera with 12-bit dynamic range and Peltier cooling (QImaging, Retiga 1300), a VariSpec liquid crystal tunable filter, an IR-cut filter, and a personal computer (see reference 21). The imaging system was placed at the same height as the target object, approximately 3 m away. The image data were represented by 61-dimensional vectors.

We selected three different objects regarded as inhomogeneous dielectric materials from the everyday objects in the experiment. Figure 9 shows a scene comprising three objects, where the left object is a blue cylinder made of painted metal, the center object is a glossy natural object, red paprika, and the right object is a yellow soy sauce container made of ceramic. These objects were placed on a black felt cloth and illuminated using three different light sources: an incandescent light source from a light bulb in the left direction, a fluorescent light source from a table lamp in the right direction, and an LED light source from a ceiling lamp in the upper direction. The image size was 638 × 884. The distances between the light sources and target objects were 1–3 m. Areas with gloss or specular highlights can be observed on the surface of each object.

The dichromatic reflection properties are well known for paints and ceramics. So we validated that the red paprika has dichromatic reflection properties. In the region surrounded by a white rectangular in Figure 9, the red paprika is illuminated only by the incandescent light from the left, and the influence of other light sources can be considered sufficiently small. We cut out the corresponding region of the spectral image and applied the singular value decomposition (SVD) to the high dimensional dataset. As a result, the cumulative contribution rate for the first two principal components was 0.988, so it was judged that the spectral dataset was two-dimensional. We next checked whether the spectral functions for the specular and diffuse components could be described using the two principal components. For this purpose, a linear combination of the two principal components needed to describe each of the illuminant spectrum $E(\lambda)$ and the diffuse reflection spectrum $S(\lambda)E(\lambda)$ was determined by a least-squares fitting. Figure 10 shows the fitting results to (A) the specular reflection component and (B) the diffuse reflection component. The broken curve in (A) represents the directly measured illuminant $E(\lambda)$ of the incandescent light source, and the bold curve represents the estimated curve by the fitting. The broken curve in (B) represents the diffuse spectrum $S(\lambda)E(\lambda)$ based on the red paprika's direct reflectance measurement, and the bold curve represents the estimated curve. The two spectral functions can be estimated using only two principal vectors. Thus, the red paprika follows the dichromatic reflection model.

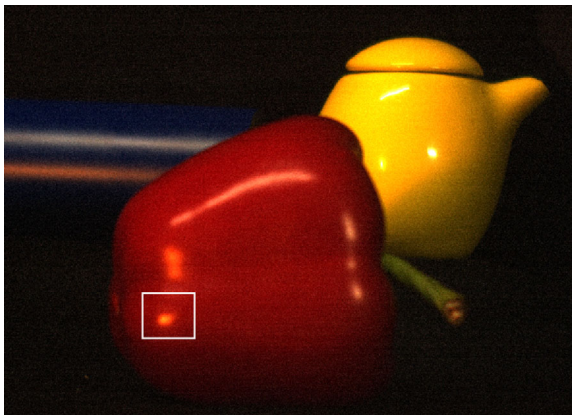

FIGURE 9 Scene comprising three objects, where the left object is a blue cylinder made of painted metal, the center object is a glossy natural object, red paprika, and the right object is a yellow soy sauce container made of ceramic.

6.2 | Illuminant estimation

The spectral image captured from the scene was converted into a luminance image to which the center-surround filter

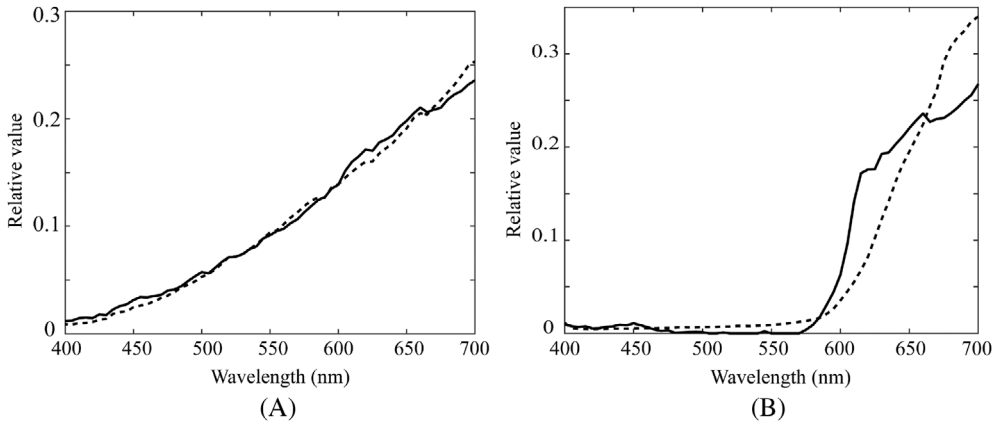

FIGURE 10 Fitting results to (A) the specular component $E(\lambda)$ and (B) the diffuse component $S(\lambda)E(\lambda)$. The broken curves in (A) and (B) represent the directly measured illuminant of the incandescent light source and the diffuse spectrum based on the direct reflectance measurement of the red paprika, respectively. The bold curves represent the estimated curves by the fitting.

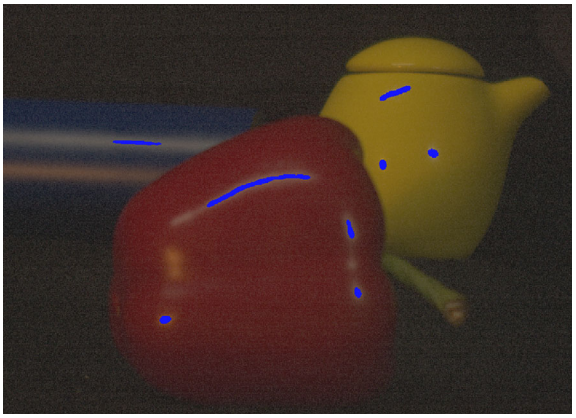

FIGURE 11 Detected highlight areas with strong intensity except for the boundary regions

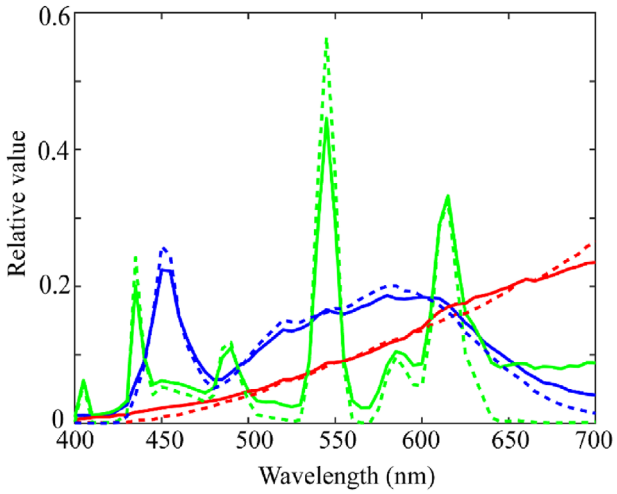

FIGURE 12 Spectral curves are estimated for three light sources, where the bold red, green, and blue curves correspond to the incandescent, fluorescent, and LED light sources' estimated illuminant spectra. The broken curves represent the directly measured illuminant spectral power distributions.

and the low pass filter were applied. The standard deviations were set to the same values as $\sigma_1 = 12$, $\sigma_2 = 3$, and $\sigma_3 = 20$ in Figure 3, and the filter sizes were $2^*\sigma_i + 1$ ($i = 1, 2, 3$). We then selected specular highlight areas with strong intensities. The blue areas in Figure 11 show the entire set of eight highlight areas extracted from the three object surfaces.

The spectral power distribution was estimated for each of the detected highlight areas. The SVD was applied to the dataset of the observed spectra at each highlight area, and the spectral data were then mapped onto a plane defined by the two singular vectors. Eight illuminant spectral curves were estimated for the eight highlight areas and the procedure described in Section 2.2. Finally, the light source for each highlight and the corresponding spectral power distribution were determined using the *k*-means clustering algorithm. Figure 12 shows the spectral curves estimated for three light sources. The three bold red, green, and blue curves correspond to incandescent, fluorescent, and LED light sources' estimated illuminant spectra. The broken curves represent the directly measured illuminant spectral power distributions.

6.3 | Reflectance estimation

The surface spectral reflectances of the respective objects in the scene shown in Figure 9 were estimated according to the algorithm proposed in Section 3. The number of light sources was $K = 3$, and the estimated spectral curves in Figure 12 were used as $\widehat{E}_i(\lambda)$ ($i = 1, 2, 3$) for reflectance estimation. We first cut out a ROI to estimate the spectral

reflectance on each object surface and determined the corresponding observed color signals $\mathbf{y}_i$ ($i = 1, 2, ..., N$). Figure 13 shows the three ROIs for the blue-painted metal, red paprika, and yellow ceramics. The number of pixels N used for the reflectance estimation was the number of pixels in each rectangular box. The number of wavelengths utilized was 61.

The spectral reflectance and shading terms in each region were estimated using an iterative estimation process. The ROI for the red paprika included strong specular highlights; therefore, the original algorithm was used. Meanwhile, the ROIs for the blue-painted metal and yellow ceramics had no highlights; thus, the simplified algorithm using Equation (14) was adopted. The number of iterations was approximately 50–100. Figure 14 shows the estimation results of spectral reflectance $\mathbf{s}$ for the three objects. The bold curves represent the estimated spectral reflectances, and the dashed curves represent the directly measured spectral reflectances by a spectrometer, which was used as the ground truth. The RMSEs for the ground truth were $rmse = 0.019$, 0.030, and 0.013 for the blue-painted metal, red paprika, and yellow ceramic, respectively. We also calculated the CIE-LAB color differences under a white illuminant with equal energy. We obtained *DE2000* values of 1.39, 5.25, and 1.81. The potential reason with such a large difference as 5.25 for the red paprika is that the selected region includes several specular highlights. Strong highlight regions tend to have large errors in spectral reflectance estimation. The spectral reflectance of red paprika can also be estimated using the matte region without highlights. The estimation results are reported in Reference 22.

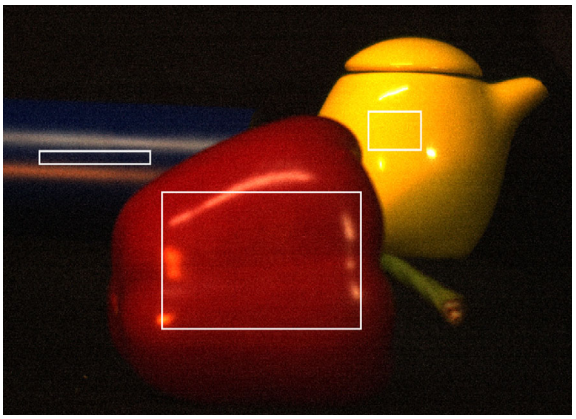

FIGURE 13 Regions of interest (ROIs) used for estimating the spectral reflectance. The rectangular boxes represent ROIs for the blue painted metal, red paprika, and yellow ceramics, from left to right.

6.4 | Shading term estimation and region segmentation

According to the algorithm in Section 4.1, the shading terms were estimated based on the previously estimated spectral functions of the illuminant and reflectance. A wide area, including both mattes and highlights, was selected as the reference region. We then calculated the reference color signal, $\mathbf{y}_{\text{ref}}$, and the SAs between $\mathbf{y}_{\text{ref}}$ and the observed color signals. We set the angle threshold to approximately 30° and detected pixels within this threshold for the same image.

Figure 15 shows the result of region segmentation, where three object regions with blue, red, and yellow colors were extracted, corresponding to the blue-painted metal, red paprika, and yellow ceramics, respectively. The estimated shading term $\hat{\mathbf{c}}(x_j)$ for each segmented region is shown in the shading images in Figure 16, where the three rows (B, R, Y) represent the blue painted metal, red paprika, and yellow ceramics objects, respectively. The six

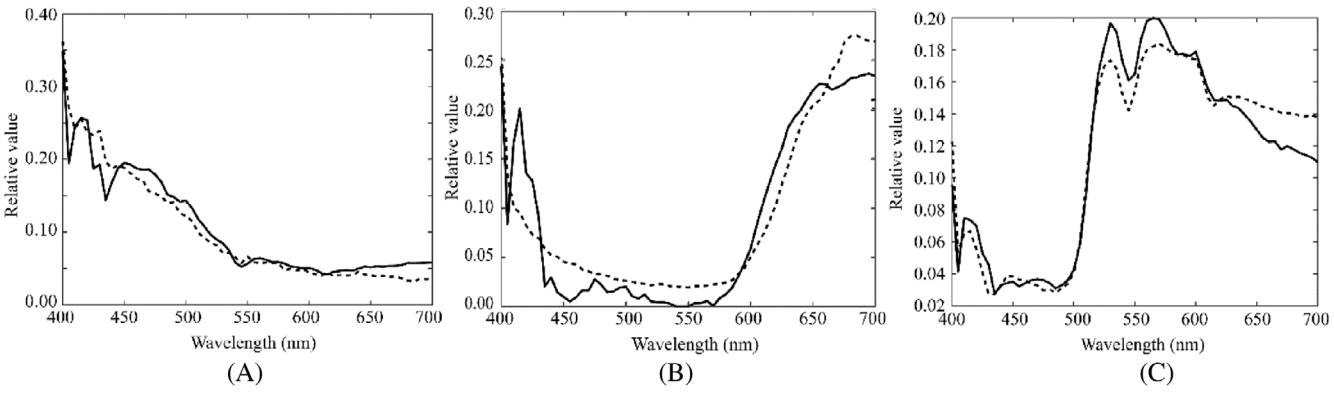

FIGURE 14 Estimation results of spectral reflectance for the three objects of (A) blue painted metal, (B) red paprika, and (C) yellow ceramics, where the bold curves represent the estimated spectral reflectances, and the dashed curves represent the directly measured spectral reflectances used as the ground truth.

columns represent $(\widehat{c}_{S1}(\mathbf{x}), \widehat{c}_{S2}(\mathbf{x}), \widehat{c}_{S3}(\mathbf{x}))$ for the specular component, and $(\widehat{c}_{D1}(\mathbf{x}), \widehat{c}_{D2}(\mathbf{x}), \widehat{c}_{D3}(\mathbf{x}))$ for the diffuse component, which were caused by three illuminations from the upper, right, and left light sources. The shaded images in the figure include shadows occluded by other objects. Shading image R6 appears very bright because the high-intensity lamp is located close to the object.

To evaluate the comprehensive accuracy of the proposed estimation approach, we calculated the RMSEs between the predicted and observed color signals using $e(\mathbf{x}) = \sqrt{\|\widehat{\mathbf{y}}(x) - \mathbf{y}(x)\|^2/61}$. Figure 17 shows the spatial distribution of the error $e(\mathbf{x})$ for the three objects, where the gray scale represents the relative magnitude of the error. It should be noted that the error distribution is not spatially constant; large errors are limited to the highlight areas, whereas the errors are small in other areas. As the intensity of the specular highlight increased, the error also tended to increase.

6.5 | Appearance reconstruction

A variety of different appearances of the objects in the scene can be constructed by modifying the two spectral functions of reflectance and illuminant, as well as the

FIGURE 15 Region segmentation result, where blue, red, and yellow regions are extracted for the blue painted metal, red paprika, and yellow ceramics, respectively.

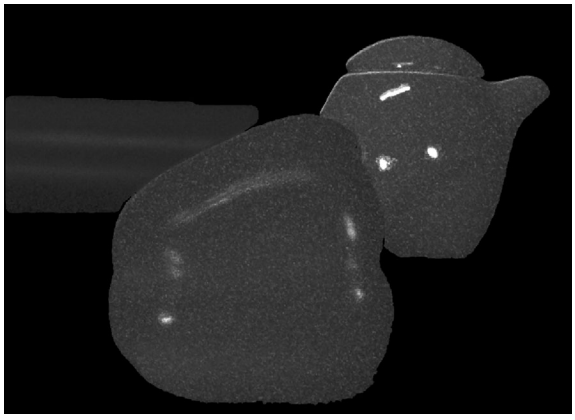

FIGURE 17 Spatial distribution of RMSEs on the three objects, where the gray scale represents the relative magnitude of the error.

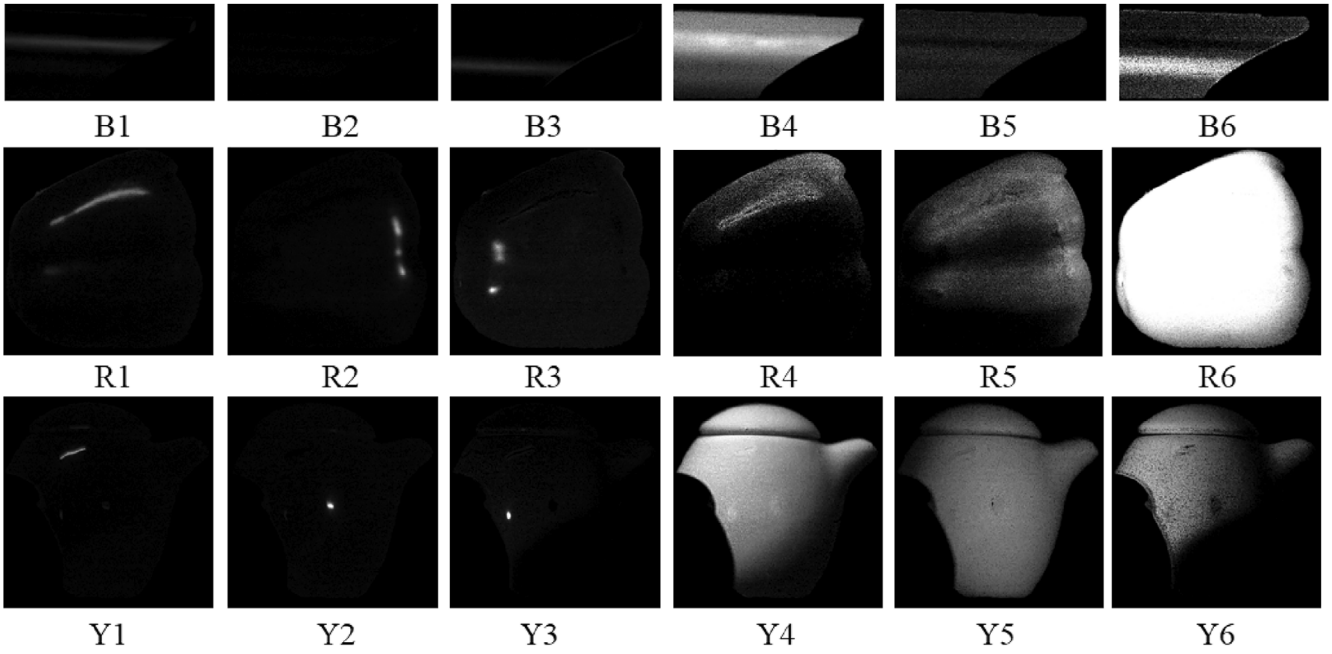

FIGURE 16 Estimated shading term for each segmented region, where the three rows (B, R, Y) represent the blue painted metal, red paprika, and yellow ceramics objects, respectively. The six columns represent the three terms 1–3 for the specular component and the three terms 4–6 for the diffuse component, which were caused by the three illuminations from the upper, right, and left light sources.

shading terms, according to the flow in Figure 8. The typical reconstruction results were obtained as follows.

First, we changed the surface spectral reflectance of the objects under the same illumination environment. Figure 18 shows the measured spectral reflectances from the three-color patches of brown, green, and pink included in an X-rite Color Checker, which were used, respectively, for the blue painted metal, the red paprika, and the yellow ceramics in the original scene. Figure 19A demonstrates a novel appearance reconstructed under the original illuminant conditions, where the object colors change, but the dichromatic reflection property does not change; thus, specular highlights are included. Figure 19B shows a novel appearance for the matte object surfaces, where the reflection has only a diffuse component and no specular component when setting $(\widehat{c}_{S1}(\mathbf{x}), \widehat{c}_{S2}(\mathbf{x}), \widehat{c}_{S3}(\mathbf{x}))$ to zeros.

Next, the illumination conditions were changed. The upper light source was neglected and the illuminant spectra of the remaining two light sources were assumed to be the CIE standard illuminant D65.[23] Figure 20A demonstrates a novel appearance for the same object surface, as shown in Figure 19A, which was illuminated with the D65 illuminant from two light sources on the left and right sides. Figure 20B shows the matte appearance without specularity. In this case, as well as in Figure 19B, the object surfaces appear matte and illuminated by diffuse light sources or nondirectional ambient light, in contrast to the directional light sources.

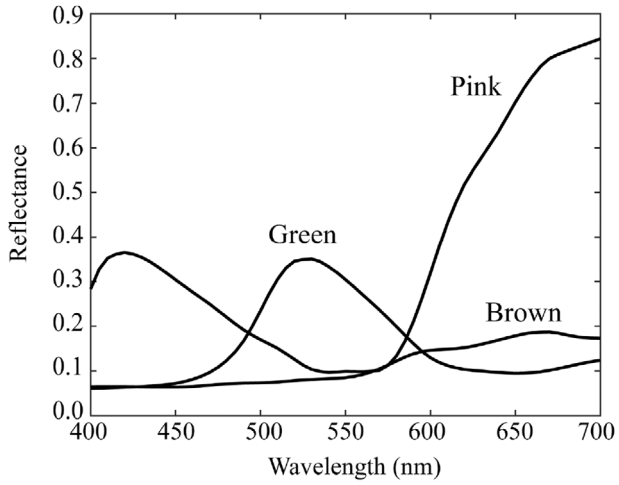

FIGURE 18 Spectral reflectances measured from the three-color patches of brown, green, and pink in an X-rite color checker, which were used, respectively, for the blue painted metal, red paprika, and yellow ceramics in the original scene.

7 | CONCLUSIONS

We proposed an approach for estimating and reconstructing the material appearance of an object based on the spectral image data acquired in a complex illumination environment with multiple light sources. The use of high-dimensional spectral spaces not only increased the accuracy of reconstruction but was also far more versatile than the use of color spaces. Object appearance can be constructed with various material properties such as

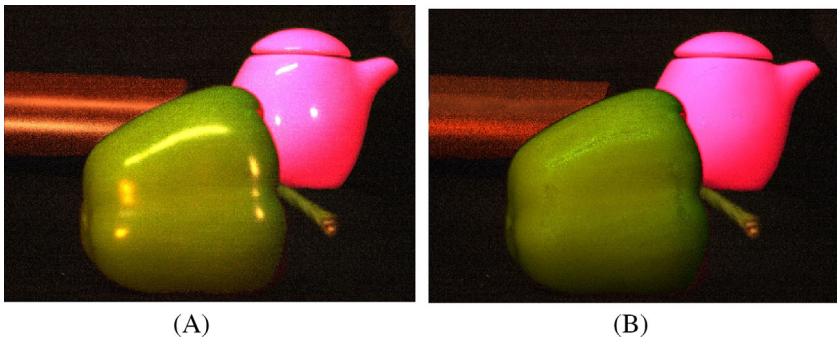

FIGURE 19 Novel appearances of the three objects reconstructed using the surface reflectances in Figure 17 under the original illuminant conditions. (A) Appearance for the gloss surfaces where the dichromatic reflection property does not change, and thus specular highlights are included. (B) Appearance for the matte surfaces without specularity.

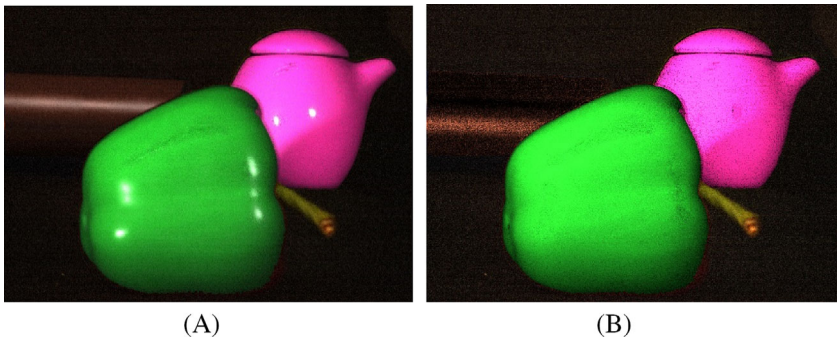

FIGURE 20 Novel appearances of the three objects reconstructed under changed illumination conditions. (A) Appearance for the gloss surfaces illuminated with the D65 illuminant from only two light sources, left and right. (B) Appearance for the matte surfaces with the same spectral reflectances without specularity under the same light sources.

spectral reflectance, glossiness, and matteness under different geometric and spectral illumination conditions.

The objects we targeted in this study were everyday objects such as natural objects and man-made objects, which were assumed to be made of an inhomogeneous dielectric material with gloss or specularity. The color signals from the object surface were described by the standard dichromatic reflection model, which consisted of two additive components, diffuse reflection and specular reflection, where the specular component had the same spectral composition as the illuminant.

The overall appearance of the objects was determined by a combination of chromatic factors based on the reflectance and illuminant spectra and the shading terms representing the surface geometries of the surface illumination. Therefore, the appearance of a novel object can be estimated and reconstructed by modifying the chromatic factors and shading terms. We present a four-step procedure for estimating and reconstructing an object appearance based on spectral image data.

First, multiple illuminants were estimated from the highlight areas on the object surfaces. Each specular highlight area corresponds to only one light source, and the detected highlight has the same spectral composition as the light source. Second, we developed an iterative algorithm that repeatedly estimates the reflectance and shading terms in two steps. This algorithm utilizes the fact that spectral reflectance and shading terms have different domains: wavelength and spatial coordinates. Third, we estimated the shading terms in a large image area and then segmented each object region using the SA, defined as the spectral similarity. Fourth, we reconstructed the novel appearances of the objects by modifying some components of the reflection model in the respective segmented regions. We presented the entire procedure for appearance reconstruction. It should be noted that the appearance of objects under different conditions can be reconstructed using only one spectral image without knowing the 3D object shape.

The proposed approach was validated in an experiment in which three objects made of different materials were observed using a spectral imaging system under three light sources with different spectra. We show the estimation results for the illuminants, reflectances, shading terms, and segmentation results. The comprehensive accuracy of the proposed approach is revealed by the spatial distribution of the RMSE between the predicted color signals and the observed image. Finally, we demonstrated typical reconstruction results with novel appearances of objects in a scene.

The image processing pipeline proposed in this article incorporated some interactive processing to improve processing efficiency and did not adopt the machine learning approach. The obstacle of the machine learning approach to the present problem is the lack of commonly used standard training datasets of spectral images, even in the image segmentation stage. There are a wide variety of spectral imaging systems with different spectral sensitivities and many light sources with different spectral distributions. Standardization of spectral image data is desired in the future.

The limitations of the method proposed in this article are summarized as follows:

1. The target material is limited to the dielectric object having the dichromatic reflection property. Therefore, the method does not apply to metal and translucent material with subsurface scattering.
2. The object shape is limited to convex. It is difficult for a concave or flat object to detect highlights and identify the light sources.
3. The reflection components are limited to the two components of diffuse reflection and specular reflection. The effect of mutual reflection is not considered.
4. Multiple light sources are supposed to be separated from the target objects also separated from each other. Therefore, if the light sources overlap, they are treated as one light source. However, if the light sources are close to each other and the object surfaces are close to flat, it is difficult to separate the light sources using the highlight areas. Moreover, when a large area light source is near the objects, highlight detection and light source identification become less accurate.
5. The image processing pipeline in the proposed method incorporates some interactive processing to improve processing efficiency so that it has partly manual inputs such as the determination of ROI. However, full automation remains as future work.

AUTHOR CONTRIBUTIONS

Shoji Tominaga: Conceptualization; Measurement and Analysis; Literature Review; Experiment; Writing draft. **Roseline Kim Fong Yong:** Conceptualization; Refine.

ACKNOWLEDGMENTS

This work was supported by Japan Society for the Promotion of Science KAKENHI Grant Number JP20K11893. The authors thank Hideaki Sakai, Professor Emeritus, Kyoto University for the useful discussions on estimation.

DATA AVAILABILITY STATEMENT

Author elects to not share data.

ORCID

Shoji Tominaga https://orcid.org/0000-0001-6460-7694

REFERENCES

[1] Carroll R, Ramamoorthi R, Agrawala M. Illumination decomposition for material recoloring with consistent interreflections. *ACM Trans Graph*. 2011;30(4):1-10.

[2] Beigpour S, van de Weijer J. Object recoloring based on intrinsic image estimation. *Proc IEEE Int Conf Comput Vis*. 2011;1:327-334.

[3] Amano T, Komura K, Sasabuchi T, Nakano S, Yamashita S. Appearance control for human material perception manipulation. *Proc Int Conf Patter Recognition*. 2012;1:13-16.

[4] Serrano A, Myszkowski K, Seidel HP, Masia B. An intuitive control space for material appearance. *ACM Trans Graphics*. 2016;35:Article 186.

[5] Katsunuma T, Hirai K, Horiuchi T. Fabric appearance control system for example-based interactive texture and color design. *ACM Trans Appl Perception*. 2017;14(3):Article 16.

[6] Manabe Y, Tanaka M, Horiuchi T. Glossy appearance editing for heterogeneous material objects. *J Imaging Sci Technol*. 2021;65(6):060406-1-060406-14.

[7] Wandell BA. *Foundations of Vision*. Sinauer Associates; 1995:290-295.

[8] Shafer S. Using color to separate reflection components. *Color Res Appl*. 1985;10:210-218.

[9] Tominaga S, Wandell B. Standard reflectance model and illuminant estimation. *J Opt Soc Am A*. 1989;6(4):576-584.

[10] Tominaga S. Surface identification using the dichromatic reflection model. *IEEE Trans Pattern Anal Mach Dermatol Int*. 1991;13(7):658-670.

[11] Tominaga S. Dichromatic reflection models for a variety of materials. *Color Res Appl*. 1994;19(4):277-285.

[12] Tominaga S, Guarnera GC. Appearance synthesis of fluorescent objects with mutual illumination effects. *Color Res Appl*. 2021;47:1-15. doi:10.1002/col.22747

[13] Tominaga S, Hirai K, Horiuchi T. Spectral estimation of multiple light sources based on highlight detection. *J Imaging Sci Technol*. 2020;64(5):50408-1-50408-9.

[14] Duda RO, Hart PE. *Pattern Classification and Scene Analysis*. John Wiley & Sons; 1973:248-267.

[15] Kruse FA, Lefkoff AB, Boardman JB, et al. The spectral image processing system (SIPS) - interactive visualization and analysis of imaging spectrometer data. *Remote Sens Environ*. 1993;44:145-163.

[16] Angelopoulou E, Lee SW, Bajcsy R. Spectral gradients: a material descriptor invariant to geometry and incident illumination. *Proc IEEE 7th Int Conf Comput Vis*. 1999;1:861-867.

[17] De Carvalho OA, Meneses PR. Spectral correlation mapper (SCM): an improvement on the spectral angle mapper (SAM). Paper presented at: 9th JPL Airborne Earth Science Workshop; 2000; 1-18; JPL Publication.

[18] Du Y, Chang CI, Ren H, Chang CC, Jensen JO, D'Amico FM. New hyperspectral discrimination measure for spectral characterization. *Opt Eng*. 2004;43(8):1777-1786.

[19] Wang K, Yong B, Gu X, Xiao P. Spectral similarity measure using frequency spectrum for hyperspectral image classification. *IEEE Trans Geosci Remote Sens Lett*. 2015;12(1):130-134.

[20] MathWorks. Interactive image inpainting using exemplar matching, https://matlab.mathworks.com/

[21] Tominaga S, Hirai K, Horiuchi T. Estimation of fluorescent Donaldson matrices using a spectral imaging system. *Opt Express*. 2018;26(2):2132-2148.

[22] Tominaga S. Spectral-reflectance estimation under multiple light sources. *Proc Color Imaging Conference*. 2021;29:25-30.

[23] Ohta N, Robertson AR. *3.9: Standard and Supplementary Illuminants, Colorimetry*. Wiley; 2005:92-96.

AUTHOR BIOGRAPHIES

Shoji Tominaga received PhD in electrical engineering from Osaka University in 1975, joined Chiba University where he was a professor (2006–2013), dean (2011–2013), a specially appointed researcher (2013–2018), and he is currently an adjunct professor at NTNU, Norway, and a visiting researcher at Nagano University, Japan. His research interests include fluorescent appearance analysis and synthesis, multispectral imaging, and material appearance. He is a life fellow IEEE, fellow IS&T, life fellow SPIE, fellow OSA, and honorary member of Color Science Association of Japan.

Roseline Kim Fong Yong received PhD in Health Science from Tokyo University in 2013 and joined Akita University as a research associate in 2015. She is also the founder of the nonprofitable organization HIKIYA (Home for Hikikomori) (since 2013), which developed into a university-originated venture business in 2022. She is an expert in social epidemiology and community mental health building, and her research interest extends to the relationship between color science, material appearance, and health.

How to cite this article: Tominaga S, Yong RKF. Appearance estimation and reconstruction of glossy object surfaces based on the dichromatic reflection model. *Color Res Appl*. 2022;47(6):1313-1329. doi:10.1002/col.22824